

# DeepGANTT: A Scalable Deep Learning Scheduler for Backscatter Networks

Daniel F. Pérez-Ramírez<sup>\*†</sup>, Carlos Pérez-Penichet<sup>\*</sup>, Nicolas Tsiftes<sup>\*</sup>, Thimo Voigt<sup>\*‡</sup>,  
Dejan Kostic<sup>\*†</sup>, Magnus Boman<sup>†</sup>

<sup>\*</sup>RISE AB, <sup>†</sup>KTH Royal Institute of Technology — Stockholm, Sweden

<sup>‡</sup>Uppsala University — Uppsala, Sweden

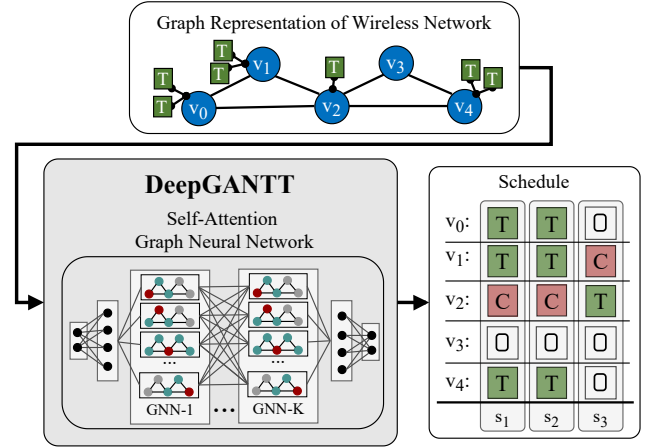
Emails: {daniel.perez, carlos.penichet, nicolas.tsiftes, thimo.voigt}@ri.se, {dmk, mab}@kth.se

**Abstract**—Recent backscatter communication techniques enable ultra low power wireless devices that operate without batteries while interoperating directly with unmodified commodity wireless devices. Commodity devices cooperate in providing the unmodulated carrier that the battery-free nodes need to communicate while collecting energy from their environment to perform sensing, computation, and communication tasks. The optimal provision of the unmodulated carrier limits the size of the network because it is an NP-hard combinatorial optimization problem. Consequently, previous works either ignore carrier optimization altogether or resort to suboptimal heuristics, wasting valuable energy and spectral resources. We present DeepGANTT, a deep learning scheduler for battery-free devices interoperating with wireless commodity ones. DeepGANTT leverages graph neural networks to overcome variable input and output size challenges inherent to this problem. We train our deep learning scheduler with optimal schedules of relatively small size obtained from a constraint optimization solver. DeepGANTT not only outperforms a carefully crafted heuristic solution but also performs within  $\sim 3\%$  of the optimal scheduler on trained problem sizes. Finally, DeepGANTT generalizes to problems four times larger than the maximum used for training, therefore breaking the scalability limitations of the optimal scheduler and paving the way for more efficient backscatter networks.

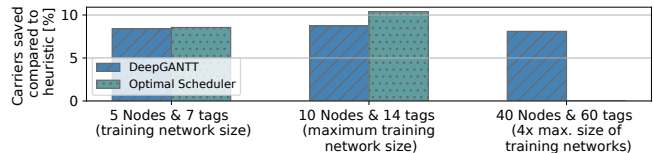
**Index Terms**—scheduling, machine learning, backscatter communications, wireless, combinatorial optimization

## I. INTRODUCTION

Backscatter communications enable new wireless devices that harvest energy from their environment to operate without batteries [1]–[3]. Recent advances have demonstrated how battery-free backscatter devices—tags for short—can seamlessly interoperate with unmodified commodity wireless devices [4]–[10]. This type of integration facilitates new applications where tags are placed in hard to reach locations where they can perform sensing, while more powerful commodity devices provide the necessary communications support from a distance [9], [10]. For backscatter tags to communicate, commodity nodes must provide an unmodulated Radio Frequency (RF) carrier. However, this comes at the cost of increased spectrum occupancy and energy expenditure for the commodity devices, which may be battery-powered. The efficient provision of unmodulated carriers is of paramount importance for system-level performance and network lifetime. We present a new scheduler called *Deep Graph Attention-based Network Time Tables* (DeepGANTT) that builds on the latest advances



(a) DeepGANTT takes a graph representing the network topology as input and produces a schedule. A schedule directs IoT nodes ( $v$ ) to interrogate every battery-free tag (T) in the network with minimal resources by reducing the number of timeslots ( $s$ ) and carrier slots (C).



(b) DeepGANTT achieves near-optimal scheduling performance and generalizes well beyond the limitation of the optimal scheduler into the range of practical network sizes. DeepGANTT’s performance is within 3% of the optimal scheduler but can be applied to up to four times larger networks.

Fig. 1: DeepGANTT employs deep learning and GNN methods to schedule wireless communications in a backscatter network. Our system performs very close to the optimal solution and applies even for problem sizes beyond those reach of the optimal scheduler used to train DeepGANTT.

in deep learning to tackle the challenging problem of efficiently scheduling the communications of battery-free tags and the supporting carrier generation in a heterogeneous network of commodity wireless devices interoperating with battery-free tags (Figure 1a).

Battery-free tags can work as sensing peripherals to augment a network of regular Internet of Things (IoT) nodes without incurring extensive maintenance and deployment costs associated with battery-powered nodes. The battery-free tags

can be located in hard-to-reach locations such as moving machinery, medical implants, or embedded in civil infrastructure. Meanwhile the more capable regular nodes are placed in accessible locations nearby, where battery replacement or mains power may be readily available [9]. The regular nodes can collect sensor readings from the tags by coordinating among themselves so that one (or more) of them provides an unmodulated carrier for its neighbors to interrogate their associated tags while avoiding collisions among carriers and data packets. Interrogating IoT devices requires a schedule that takes into account the network topology and coordinates carrier-generating and interrogating devices to query all tags. Because the IoT nodes invest significant energy and spectral resources interrogating the tags, it is important to schedule as many tag interrogations as possible with every unmodulated carrier generated, and to do so in as few timeslots as possible.

**Challenges.** Computing the optimal schedule is an NP-hard combinatorial optimization problem. The only known scalable solution is a heuristic with suboptimal performance [11], which results in wasted energy and spectral resources. We will refer to this suboptimal solution as *the TagAlong scheduler* [10] hereafter. It is possible to compute optimal solutions using a constraint optimization solver, but only for small problem instances as it takes a prohibitively long time for more practical network sizes (schedules for 10 nodes and 14 tags can take a few hours). We will refer to the scheduler based on the constraint solver as *the optimal scheduler*. With DeepGANTT, we leverage deep learning methods to overcome both the scalability limitations of the optimal scheduler and the performance shortcomings of the TagAlong scheduler.

From the deep learning point of view, the tag scheduling problem presents two significant challenges: First, traditional deep learning methods that have succeeded greatly on problems with fixed input and output size (such as computer vision and tabular data) are not applicable to our scheduling problem given that both the input and output sizes depend on the number of IoT devices and sensor tags. Second, every problem instance (of sufficient size) has a large number of equivalent optimal solutions and this could confuse Machine Learning (ML) models in training. This is due to many symmetries resulting from the problem formulation, e.g., that all schedules are invariant to timeslot permutations, among others.

**Approach.** DeepGANTT takes the network’s topology graph as input and generates a corresponding interrogation schedule (Figure 1a). We adopt a supervised learning deep neural network approach instead of other paradigms such as reinforcement learning. This choice is mainly motivated by two facts. First, we can leverage the optimal scheduler to produce a training set necessary for a supervised approach. Second, it is straightforward to cast the scheduling problem as a classification problem, which is generally tackled with a supervised approach.

DeepGANTT performs node classification on every IoT node to predict the role each of them will play within every schedule timeslot: remain off (O), interrogate a tag (T) or

generate a carrier (C). We seek to obtain the shortest possible schedule with the fewest number of carrier generation (C) slots. We train DeepGANTT with the optimal solutions to randomly generated problem instances of relatively small size obtained with the optimal scheduler. To address the challenge of multiple optimal solutions, we add soft constraints to the original scheduling problem intended solely to eliminate all symmetries, therefore forcing the problem to have a unique optimal solution equivalent to the original problem. We generate random problem instances of small enough size to practically compute optimal solutions using a constraint optimization solver. This is the training set we employ to train DeepGANTT.

**Contributions.** We introduce DeepGANTT, a fast scheduler that builds on state-of-the-art in deep learning and Graph Neural Networks (GNN) to obtain near-optimal backscatter tag interrogation schedules in a scalable manner. We show that our scheduler outperforms TagAlong (a carefully crafted heuristic solution) with a reduction of up to 50% in the number of carriers, and performs on average within 3% of the optimal scheduler on the problem sizes used for training. DeepGANTT generalizes to problems four times larger than the maximum used for training (Figure 1b), therefore breaking the scalability barrier of the optimal scheduler. As a consequence, DeepGANTT enables significant energy and spectrum savings in backscatter networks. Finally, our scheduler achieves all this with an inference time that is always below 1.5s and on average is 429ms for the largest size, a radical improvement over the optimal scheduler.

We make the following specific contributions:

- We leverage state-of-the-art GNN techniques to overcome the limitations of traditional deep learning approaches regarding the variable input and output size of our scheduling problem. We also address the proper choice of the loss and activation functions as well as the structural components of the model.
- Crucially, we leverage symmetry-breaking constraints to limit the solution space of the scheduling problem, therefore avoiding the pitfalls caused during training by the multiplicity of solutions.
- We present DeepGANTT, a deep learning scheduler that scales up to four times larger problem sizes than the optimal scheduler while achieving performance within 3% of the optimum.

## II. SYSTEM MODEL

The DeepGANTT scheduler is designed to operate in the context of a wireless network of commodity IoT devices that has been augmented with a set of battery-free tags. The tags achieve the necessary low power consumption to operate without batteries by a combination of backscatter and related techniques [9], [10], [12]. For battery-free tags to send and receive information from an IoT node, they require an external RF signal—an unmodulated carrier—provided by a second IoT node. Every tag is associated with (or hosted by) one IoT device responsible for collecting its sensor readings.

Every IoT node in the network may host zero or more tags. The IoT devices in the network are equipped with radio transceivers that support standard physical layer protocols such as IEEE 802.15.4 or Bluetooth. They are able to provide an unmodulated carrier (by using their radio test mode [9]) and employ a time-slotted medium access mechanism. The duration of a timeslot is sufficient for an IoT device to interrogate one tag by transmitting a request to the desired tag and receiving the response a short interval after while a second IoT node provides an unmodulated carrier, as demonstrated by Pérez-Penichet et al. [10], [11]. Note that both IEEE 802.15.4 and Bluetooth specify a time-slotted access mechanism with the necessary characteristics in their respective standards [13], [14]. Finally, at least one of the IoT devices is connected to a cloud or edge server where the interrogation schedule can be computed.

The network of IoT nodes has the ability to collect link state information to determine the connectivity graph among themselves. This information is relayed to the cloud server, where it is, together with the tag-to-host mapping, used to assemble the graph representation of the network. Our scheduler uses this graph representation to produce a schedule, as depicted in Figure 1a. An interrogation schedule consists of one or more scheduling *timeslots*, each assigning one of three roles to every IoT device in the network (Figure 1a): Provide an unmodulated carrier (C), interrogate a sensor tag (T), or remain idle (0). The goal of the scheduler is to generate an interrogation schedule that queries all tags while requiring as few carrier generation slots and timeslots as possible. The number of carriers is the most important aspect affecting the overall spectral efficiency and energy consumption of the system.

**Schedule constraints.** The properties of backscatter communication impose physical constraints on the way tags are interrogated. First, within a timeslot, a tag can be interrogated by its host iff exactly one of its neighboring IoT devices provides an unmodulated carrier. Multiple incoming unmodulated carriers may cause disrupt the tag-to-host communication [10]. Similarly, the limited communication range of the battery-free tags forces them to be interrogated exclusively by their hosts, which must be located nearby. Note that timeslots are permutation invariant, which implies that one can arbitrarily shuffle the order in which the timeslots appear in the schedule. Because of this and other symmetries, the scheduling problem typically has multiple optimal solutions.

### III. PROBLEM FORMULATION

For the scheduler, the goal is to find a feasible interrogation schedule for the IoT devices to query all tags using as few timeslots and carrier generators as possible. We hereon refer to the IoT devices and to the sensor tags in the network as *nodes* and *tags*, respectively. We model the wireless IoT network as an undirected connected graph  $G$ , defined by the tuple  $G = \langle V_a, E \rangle$ , where  $V_a$  is the set of  $N$  nodes in the network  $V_a = \{v_i\}_{i=0}^{N-1}$ , and  $E$  is the set of edges between the nodes  $E = \{\langle u, v \rangle | u, v \in V_a\}$ . The graph is built such that there is an edge between nodes iff there is a sufficiently strong wireless signal

for providing the unmodulated carrier. Furthermore, we denote the set of  $T$  tags in the network as  $N_t = \{t_i\}_{i=0}^{T-1}$ , and their respective tag-to-host assignment as  $H_t : t \in N_t \mapsto v \in V_a$ . The role of a node  $v$  within a timeslot  $s$  is indicated by the map  $R_{v,s} : v \in V_a, s \in [1, L] \mapsto \{C, T, 0\}$ , where  $L$  is the schedule length in timeslots. Hence, a timeslot  $s_j$  consists of an  $N$ -dimensional vector containing the roles assigned to every node during timeslot number  $j$ :  $s_j = [R_{v_i,j} | v_i \in V_a]^\top$ .

For a given problem instance defined by the tuple  $g = (G, N_t, H_t)$ , the Combinatorial Optimization Problem (COP) of interrogating all sensor values in the network once using the lowest number of carrier generators and timeslots is formulated as follows:

$$\min (L^g, C^g) \quad (1)$$

$$\text{s.t. } \forall t \in N_t \exists! s \in [1, L^g] : R_{H_t, s}^g = T \quad (2)$$

$$\forall s \in [1, L^g] \forall t \in N_t | R_{H_t, s}^g = T \quad (3)$$

$$\exists! v_j \in V_a : R_{v_j, s}^g = C \wedge (H_t, v_j) \in E,$$

where  $C^g$  is the total number of carriers required in the schedule, i.e.,  $C = \left| \{R_{v_j, s}^g = C : v_j \in V_a, \hat{s} \in [1, L^g]\} \right|$ . Constraints (2) and (3) enforce that tags are interrogated only once in the schedule and that there is only one carrier-providing neighbor per tag in each timeslot, respectively. Solving (1)-(3) for a problem instance  $g$  results in the optimal schedule  $S^g$ , which corresponds to the union of all timeslots as  $S^g = \{s_j^g\}_{j=1}^{L^g} = \left\{ [R_{v_i, j}^g | v_i \in V_a^g]^\top \right\}_{j=1}^{L^g}$ .

### IV. DEEPGANTT DESIGN

In this section, we describe the key characteristics of DeepGANTT. We use a constraint optimizer to compute provably optimal solutions for small-sized problem instances, on which we train DeepGANTT. We then deploy DeepGANTT to compute interrogation schedules for unseen problem instances.

#### A. Design Considerations

We deploy DeepGANTT at an edge or cloud server where schedules are computed on demand for the IoT nodes. DeepGANTT receives a representation of the wireless network as the tuple  $g = (G, N_t, H_t)$ , i.e., the topological information of the network  $G$  in terms of IoT devices and their connectivity, the set of tags  $N_t$  in the network, and their respective tag-to-host assignment  $H_t$ . It then generates the interrogation schedule  $S^g$  and delivers it to the IoT network. DeepGANTT may receive subsequent schedule requests upon changes of either  $G$  or  $(N_t, H_t)$  due to the addition or removal of nodes and tags or connectivity changes among IoT nodes.

From an ML perspective, every possible configuration of  $g$  yields a different graph representation with different connectivity and potentially different input size. Likewise, the output may vary in size  $S^g = \{s_j^g\}_{j=1}^{L^g}$  in terms of both number of timeslots  $L^g$  and number of nodes  $N = |V_a|$  in the topology (since  $s_j^g \in \mathbb{R}^N$ ). Moreover, at every timeslot  $s_j^g$ , every node is assigned to one of three possible actions  $\{C, T, 0\}$  (see Sec. II) based on its close-proximity neighborhood. Among ML methods, GNNs are a strong candidate to serve as learning

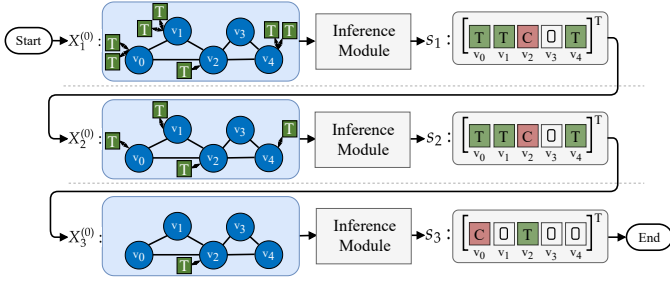


Fig. 2: DeepGANTT iteratively performs node classification on every node, one timeslot at a time, removing scheduled tags from the topology and repeating the process until no more tags remain.

basis by allowing to process variable-sized input and output sequences and by learning the local dependencies of a node through inductive learning. By using GNNs, we avoid training separate inference models to handle every possible input-output size configuration.

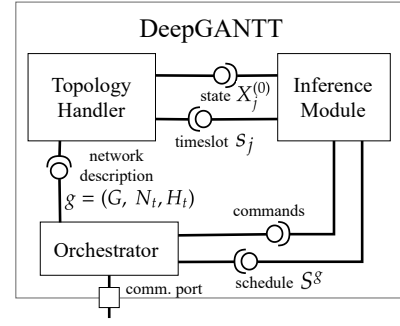
### B. System Architecture

The properties of the problem allows it to be modeled as an iterative per-node multi-class classification problem. The inner-workings of DeepGANTT is illustrated in Fig. 2: on each iteration  $j$ , the inference module of DeepGANTT assigns each node in the topology to one of three classes corresponding to the possible node actions  $\{C, T, O\}$ . Hence, each iteration  $j$  delivers the timeslot  $s_j = [R_{v_i,j} | v_i \in V_a]^T \in \mathbb{R}^N$ . After each classification procedure at  $j$ , the topology's tags-per-node information is updated by removing one tag of the nodes that were assigned class T (interrogate). The process is repeated until all tags have been scheduled.

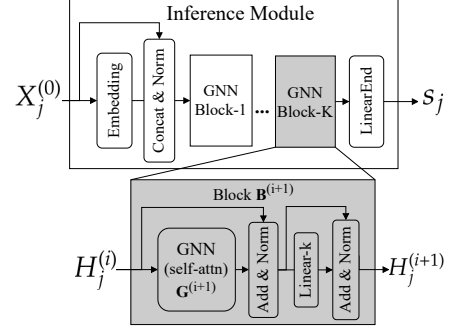
DeepGANTT consists of three submodules, as depicted in Fig. 3a. The *Orchestrator* is the coordinating unit of DeepGANTT and interacts with the outside world through its communication port. It is responsible for providing the problem description to the *Topology Handler* and interfacing with the *Inference Module*. The *Topology Handler* maintains the problem description, provides it to the *Inference Module* in a suitable format to be processed in the ML model, and updates its state according to the predicted timeslots. Since the *Inference Module*, being an ML model, is trained on the basis of a stochastic process, the *Topology Handler* includes a fail-safe functionality to confirm that the predictions comply with the constraints in Eqs. (2) and (3).

### C. Inference Module

The Inference Module is the central learning component of DeepGANTT and contains the ML model for performing inference. At timeslot  $j \in [1, L]$ , the Inference Model receives as input a node feature matrix  $X_j^{(0)} \in \mathbb{R}^{N \times D}$  containing the row-ordered node feature vectors  $x_{i,j}^{(0)} \in \mathbb{R}^D, \forall i \in V_a$ , where  $D$  represents the number of features chosen to represent a node's initial state. Since the tags lie in the immediate proximity of a node and communicate only with their host, we model them as a feature in their host's feature vector, indicating the number of tags the node hosts before timeslot  $j$ .



(a) The three core components of DeepGANTT interact among themselves and with the exterior to generate schedules.



(b) At the core of the inference module there are  $K$  GNN layers with self attention. The Inference Module is the main component where DeepGANTT performs inference.

Fig. 3: DeepGANTT is composed of three main components. The Inference Module contains the ML model. The three components interact with each other to generate schedules.

The edges in the graph correspond to the connectivity of the wireless network in terms of the ability of a node to provide a carrier to its neighbors. In the following, we describe in detail the elements of the inference module. The Inference Module consists of three parts, as depicted in Fig. 3b.

1) *Embedding*: The node feature matrix  $X_j^{(0)}$  is initially transformed by an *Embedding* component as:

$$H_j^{(0)} = \text{LN} \left( \left\| \left[ X_j^{(0)}, \text{FNN}_e \left( X_j^{(0)} \right) \right] \right\| \right), \quad (4)$$

where LN corresponds to the layer normalization operation from Ba et al. [15], and  $\|$  represents the concatenation operation.  $\text{FNN}_e$  corresponds to a fully-connected neural network layer (FCNN) with a non-linear transformation as:

$$\text{FNN}_e(X_j^{(0)}) = \text{LeLU} \left( \text{FCNN}_e(X_j^{(0)}) \right) \quad (5)$$

$$\text{FCNN}_e(X_j^{(0)}) = X_j^{(0)} W_e + b_e, \quad (6)$$

with the leaky ReLU operator LeLU and NN parameters  $W_e \in \mathbb{R}^{D \times D_e}, b_e \in \mathbb{R}^{D_e}$ , with  $D_e$  as the embedding output dimension. The motivation behind the embedding part is to assist the subsequent message-passing operations in performing injective neighborhood aggregation, while allowing the model to save a node's structural properties.

2) *Stacked GNN Blocks*: The output from the embedding component  $H_j^{(0)} \in \mathbb{R}^{|V_a| \times (D+D_e)}$  represents the input to a stack of  $K$  GNN blocks  $\{B^{(i+1)}\}_{i=0}^{K-1}$  (see Fig. 3b), each performing the following operations:

$$H_j^{(i+1)} = \mathbf{B}^{(i+1)}(H_j^{(i)}) \quad (7)$$

$$\mathbf{B}^{(i+1)}(H_j^{(i)}) = \text{LN} \left( \tilde{H}_j^{(i+1)} + \text{FNN}_B^{(i+1)} \left( \tilde{H}_j^{(i+1)} \right) \right) \quad (8)$$

$$\tilde{H}_j^{(i+1)} = \text{LN} \left( H_j^{(i)} + \mathbf{G}^{(i+1)}(H_j^{(i)}) \right), \quad (9)$$

with  $\text{FNN}_B^{(i+1)}$  as a per-node FCNN with parameters  $\{W_b^{(i+1)}, b_b^{(i+1)}\}$  (analogous to Eq. 6) followed by a leaky-ReLU. The operation  $\mathbf{G}^{(i+1)}(H_j^{(i)})$  represents a scaled dot-product multi-head self-attention GNN layer [16], [17]. Each of the  $N$  row-ordered node feature vectors  $H_j^{(i)} = \{h_{j,t}^{(i)}\}_{t=0}^{N-1}$  is updated at GNN layer  $\mathbf{G}^{(i+1)}$  with the following message-passing operation:

$$h_{j,t}^{(i+1)} = \tilde{h}_{j,t}^{(i+1)} + \prod_{m=1}^M \left[ \sum_{p \in \mathcal{N}(t)} \alpha_{m,tp}^{(i+1)} \tilde{v}_{j,m,p}^{(i+1)} \right] \quad (10)$$

$$\tilde{h}_{j,t}^{(i+1)} = \text{FCNN}_{\text{upt}}^{(i+1)} \left( h_{j,i}^{(i)} \right) = W_{\text{upt}}^{(i+1)} h_{j,t}^{(i)} + b_{\text{upt}}^{(i+1)} \quad (11)$$

$$\tilde{v}_{j,m,t}^{(i+1)} = \text{FCNN}_{m,\text{val}}^{(i+1)} \left( h_{j,t}^{(i)} \right) = W_{m,v}^{(i+1)} h_{j,t}^{(i)} + b_{m,v}^{(i+1)} \quad (12)$$

$$\alpha_{m,tp}^{(i+1)} = \frac{\Gamma \left( q_{j,m,t}^{(i+1)}, k_{j,m,p}^{(i+1)} \right)}{\sum_{u \in \mathcal{N}(t)} \Gamma \left( q_{j,m,t}^{(i+1)}, k_{j,m,u}^{(i+1)} \right)} \quad (13)$$

$$q_{j,m,t}^{(i+1)} = \text{FCNN}_{m,\text{qry}}^{(i+1)} \left( h_{j,t}^{(i)} \right) = W_{m,q}^{(i+1)} h_{j,t}^{(i)} + b_{m,q}^{(i+1)} \quad (14)$$

$$k_{j,m,t}^{(i+1)} = \text{FCNN}_{m,\text{key}}^{(i+1)} \left( h_{j,t}^{(i)} \right) = W_{m,k}^{(i+1)} h_{j,t}^{(i)} + b_{m,k}^{(i+1)} \quad (15)$$

$$\Gamma(A, B) = \frac{\exp(A^T B)}{\sqrt{d}}, \quad A, B \in \mathbb{R}^d. \quad (16)$$

Eq. 10 is the main node update operation. A node's feature vector is transformed by the update layer  $\text{FCNN}_{\text{upt}}^{(i+1)}$  in Eq. 11 and added to the concatenated  $M$ -heads of the attention operations. Each self-attention operation  $m$  consists of a weighted sum over neighboring node feature vectors, equivalent to the key-query-value operations presented by Vaswani et al. [16]. First, the neighbors' node feature vectors are transformed by the layer  $\text{FCNN}_{m,\text{val}}^{(i+1)}$  in Eq. 12. The weights  $\alpha_{m,tp}^{(i+1)}$  at attention head  $m$  from neighbor source  $p$  to target update node  $t$  are obtained through a Softmax in Eq. 13 over the scaled dot product operation  $\Gamma$  (see Eq. 16) between query  $q_{j,m,t}^{(i+1)}$  and key  $k_{j,m,t}^{(i+1)}$  vectors. The query and key vectors are obtained by the transformations  $\text{FCNN}_{m,\text{qry}}^{(i+1)}$  and  $\text{FCNN}_{m,\text{key}}^{(i+1)}$  of the target node (see Eq. 14) and the source neighbor node (see Eq. 15).

Given the structure of the message-passing operations, every GNN block allows a node to receive information from its one-hop neighborhood. Hence,  $K$ -different stacked blocks allow to node to receive input from  $K$  transformed neighborhoods. We choose summation as aggregation operation (see Eq. 10) motivated by the results of Hamilton et al. [18].

There are multiple reasons motivating the implementation of different self-attention mechanisms at each GNN block. First, attention allows to leverage neighbor contributions differently, which is specially beneficial when lacking edge weights in the network description. Second, attention has provided better results for node classification tasks [19] compared to isotropic GNNs [18], [20]. Moreover, conventional GNN node classification benchmarks assume that nodes in a spatial locality of the graph assume similar labels and leverage the fixed-point theorem property in stacking GNNs [20]. This greatly contrasts with the carrier scheduling problem, in which neighboring nodes are mostly expected to have different classes (a node provides a carrier, neighbors interrogate tags). Finally, attention serves as a counteracting factor for this property when combined with skip-connections: it builds deeper networks that can learn contrasting representations at each layer.

3) *Classification Layer*: the output from the  $K$  GNN blocks is then fed to a FCNN followed by a Softmax for obtaining a per-node probability distribution over the classes that correspond to the possible node actions  $\{\mathbf{C}, \mathbf{T}, \mathbf{0}\}$ .

Note that all parameters from the Inference Module listed (Eqs. 4–15) are shared across timeslots  $s_j$ .

## V. LEARNING INTERROGATION SCHEDULES

A supervised deep learning model, especially a GNN, is highly dependent on both the underlying data generation procedure and the chosen data representation for inference. Hence, in this section, we first explore the influence that different data-generation strategies and different node feature representations have on the performance of the Inference Module in terms of classification metrics and its ability to produce correct interrogation schedules. We then fix the data-generation strategy and feature representation to evaluate the influence of the number of GNN blocks on performance.

### A. Candidate Strategies for Data Generation

In the following, we describe the data-generation strategies implemented, to subsequently analyze their influence on the ML model performance.

1) *Simple strategy*: we configure the constraint optimizer to solve Eqs. 1 - 3 as described in Sec. III. Since the schedule, in general, is permutation invariant, the order in which the timeslots occur is irrelevant. This implies that, given a provably optimal schedule  $S^g = \{s_j^g\}_{j=1}^{L^g}$ , there are  $L^g!$  possible valid orders in which the individual scheduling timeslots can occur. For the optimal solver, this implies that the possible candidate solutions during search are highly symmetrical. Consider, e.g., a four-node star topology with a tag at its center node: this leaves three equally fitted nodes for carrier provisioning.

2) *Greedy strategy*: we start with the *Simple* strategy and add one additional soft constraint to the problem formulation. The motivation behind the additional constraint is to assist the constraint optimizer in breaking as many symmetries of the candidate solutions as possible when searching for the optimal solution. Compared to the *Simple* strategy, we add

the following components to the objective function in the constraint solver configuration:

$$\min \left( \beta_n \sum_{v \in \tilde{V}_a} \text{id}(v) \right) : \tilde{V}_a = \{v \mid R_{v,\bar{s}} = \mathbf{C} \forall \bar{s} \in [1, L]\} \quad (17)$$

$$\min \left( \beta_s \sum_{\bar{s} \in \tilde{S}} \bar{s} \right) : \tilde{S} = \{\bar{s} \mid R_{H_t,\bar{s}} = \mathbf{T} \forall t \in N_t\} \quad (18)$$

where  $\text{id}(v)$  is a function that provides the ID of node  $v$ . The purpose of Eq. 17 is to minimize the sum of the IDs from the carrier-providing nodes in the schedule. This implies that nodes with lower IDs are preferred to provide carriers to neighboring nodes. Additionally, Eq. 18 considers the sum of the timeslot numbers  $\bar{s}$  at which each tag is interrogated. This implies that the schedule favors interrogating as many tags as early as possible in the first scheduling timeslots. The scaling factors  $\beta_n$  and  $\beta_s$  control the contributions of the respective term to the overall optimization objective.

3) *Unique strategy*: we leverage the tags present in the topology as an additional element to further break the symmetries of candidate solutions by assigning sequential integer IDs to each tag in the network randomly. The *Tag-ID Strategy* encompasses the *Greedy* one, but modifies Eq. 18 to explicitly consider the tag-IDs as:

$$\min \left( \sum_{t \in N_t} s T^{T-t} \right) : R_{H_t,s} = \mathbf{T} \forall t \in N_t, s \in [1, L], \quad (19)$$

where  $T$  corresponds to the number of tags in the network  $|N_t| = T$ . The added objective from Eq. 19 represents a number of base- $T$  that has as many digits as tags in the network, and where the timeslot  $s$  at which tag  $t$  is interrogated is located at the  $t$ -significant position of the number.

### B. Candidate Initial Node Feature Representation

In this section, we describe the features used to represent the initial node features  $X^{(0)}$  (input to the Inference Module). We use different configurations of the following node features:

1) *Tags-hosted*: indicates the number of tags hosted by a node. To remain invariant to the maximum number of tags per node seen during training (in contrast to using the model on deployment), we normalize this feature in the range  $[0, 1]$  by dividing it by the maximum number of hosted tags by a node.

2) *Nodes-ID*: indicates the ID of a node. If not provided a priori, it can be randomly assigned to a node before inference. For this feature to remain invariant to the training graph sizes (in terms of the number of nodes in the graph), we normalize this feature in the range  $[0, 1]$  by dividing each nodes' Node-ID by the total number of nodes  $N$  in the topology.

3) *Min. Tag-ID*: indicates the ID of a tag. If no Tag-ID assignment is provided a priori, IDs can be randomly assigned to tags analogous to the node IDs. Since a node can host several tags, a node's Tag-ID feature represents only the lowest Tag-ID value among its hosted tags. To remain

invariant to the maximum number of tags in the network, we also normalize this feature in the range  $[0, 1]$  by performing min-max normalization among all nodes' Tag-ID values.

Based on these features, we create three different representations for  $X_j^{(0)}$ : *Feats-1* includes only the *Tags-hosted* feature ( $X_j^{(0)} \in \mathbb{R}^{N \times 1}$ ), *Feats-2* considers Feats-1 plus the *Nodes-ID* feature ( $X_j^{(0)} \in \mathbb{R}^{N \times 2}$ ), and *Feats-3* considers Feats-2 plus the *Min. Tags-ID* feature ( $X_j^{(0)} \in \mathbb{R}^{N \times 3}$ ).

### C. Implementation

We refer to small-sized problem instances to graphs having two to ten nodes ( $N \in [2, 10]$ ), and one to 14 tags ( $T \in [1, 14]$ ). We generate the graphs using the random graph generator from NetworkX [21], and assign tags to hosts by sampling node-IDs from a uniform distribution. We generate solutions for a total of 520K problem instances for each of the three data-generation strategies in Sec. V-A using MiniZinc [22] (*Simple* strategy) and OR-Tools [23] (*Greedy* and *Unique* strategies). The problem instances are split into a train- and a test-set. Since we perform a per-node classification for every scheduling timeslot (see Fig 2), we consider each timeslot input-target pair  $(X_j^{(0)}, s_j)$  as a training sample, which yields an approximate total of 1.5M samples. We instantiate the Inference Module using PyTorch [24], whereas for the GNNs layers  $\mathbf{G}^{(i+1)}$  we use the PyTorch-Geometric self-attention based GNN *TransformerConv* implementation [25].

### D. Training and ML Model Evaluation

For training we use a 20-80 test-train set split of the problem instances. We train the Inference Module with the Adam optimizer [26] on the basis of mini-batch gradient descent with standard optimizer parameters and an initial learning rate of  $10^{-3}$ . As loss function, we propose a modified version of the multi-class cross-entropy:

$$L_{batch} = \frac{1}{N_b} \sum_{\hat{y}=0}^{N_b-1} L_x(\hat{y}, y) L_1(\hat{y}, y) \quad (20)$$

$$L_x(\hat{y}, y) = - \sum_{k \in \{C, T/O\}} y_k \log(\hat{y}_k) + \rho \|\hat{W}\|_2^2 \quad (21)$$

$$L_1(\hat{y}, y) = \exp(|(\hat{y} == \mathbf{C}) - (y == \mathbf{C})|), \quad (22)$$

where  $N_b$  is the number of nodes in the mini-batch,  $\rho$  is the regularization hyperparameter, and  $\hat{W}$  represents the tensor containing all the learning parameters undergoing gradient descent. We implement learning rate decay by 10% every five epochs, and early stopping after 25 subsequent epochs without minimization of the test-loss. We save the best performing model on the basis of the F1-score.

### E. Evaluation Metrics

We consider both ML metrics and an application-related metric to evaluate a model's performance. From the ML perspective, we employ overall accuracy and the carrier class C F1-score. For the application-related metric we consider the percentage of correctly computed schedules  $S_{corr}$ . This metric

TABLE I: *The characteristic of the training data and the node features strongly impact the model’s performance. The modified scheduling problem with unique solutions dramatically improves the quality of the model.* Influence of data-generation strategies and node feature representation for an Inference Module of six GNN-Blocks.  $S_{corr}$  indicates percentage of problem instances for which the NN delivers a complete schedule. F1-score is provided for C (carrier class).

Data-generation strategy: Perf. Metric [%]:	Simple			Greedy			Unique		
	Accuracy	F1-score	$S_{corr}$	Accuracy	F1-score	$S_{corr}$	Accuracy	F1-Score	$S_{corr}$
Feats-1 ( $D = 1$ ):	85.69	57.78	27.04	87.88	63.78	11.30	86.61	60.54	10.11
Feats-2 ( $D = 2$ ):	86.11	58.53	39.00	97.20	91.12	97.60	95.04	84.29	88.11
Feats-3 ( $D = 3$ ):	86.40	59.82	47.96	97.24	91.24	94.66	<b>99.22</b>	<b>97.36</b>	<b>99.64</b>

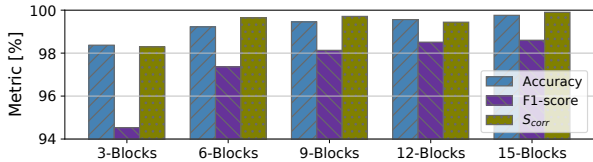


Fig. 4: *Increasing the number of GNN-Blocks improves the performance of the NN model.* Influence of the number of GNN-blocks on performance. The NN reaches a saturation point for the F1-score at approx. 12 layers.

indicates the percentage of problem instances for which the already-trained ML model produces a complete (all timeslots) and correct (fulfilling carrier scheduling constraints) schedule for the test-set’s problem instances.

#### F. Results: Influence of Data-Generation Strategy and Node Feature Representation

The considered Inference Module for evaluating data-generation strategies and node feature representation consists of six GNN-blocks. The chosen number of GNN-blocks for this experiments was empirically determined based on a trade-off between model training time and model performance.

The influence of both node feature representation and data-generation strategy in model performance is depicted in Table I. Overall, an enriched node feature representation (transitioning from Feats-1 to Feats-3) leads to an increase of the accuracy and F1-score, irrespective of the data-generation strategy. There are two possible reasons for this. First, by increasing the node feature dimension  $D$ , we ensure that the GNNs can perform more efficient injective neighborhood aggregation (to better distinguish neighboring node contributions). Second, both the Nodes-ID and Tags-ID feature serve as a node’s positional encoding information in a graph, a property that assists the model in breaking graph symmetries [27], [28].

Additionally, an enriched node feature representation greatly leads to an increase of  $S_{corr}$ , especially for the strategies Greedy (86.3% increase from Feats-1 to Feats-2) and Unique (89.5% increase from Feats-1 to Feats-3). The constraint optimizer explicitly uses the Node-ID (Greedy and Unique) and Tag-ID (Unique) to compute the optimal solution, which is why providing the NN with these features for the respective case is beneficial. Implementing symmetry-breaking measurements in the data-generation procedure is a critical measure for allowing the NN model to generate complete schedules (highest increase in  $S_{corr}$ ). Since we explore a supervised learning approach, it is of the utmost importance to limit the mapping between inputs and targets for the NN model to learn consistent topological structural dependencies.

**Features and dataset selection.** Based on the previous findings, we will set the data-generation strategy to *Unique* and the feature representation to *Feats-3* from now on.

#### G. Results: Influence of Number of GNN-Blocks

We analyze the performance of the NN model as we vary the number of GNN-Blocks, while keeping other architectural components constant on values found by extensive empirical analysis. Specifically, we set the embedding dimension to  $D_e = 48$ , the number of attention heads to  $M = 2$  and the GNN-Blocks’ hidden feature dimensions to  $D_H^{(i)} = 200$ . Fig. 4 illustrates how increasing the number of GNN-Blocks increases the performance of the NN model. We observe the F1-score increase to a saturation point around 12 layers. Although the 15-layer model exhibits the highest  $S_{corr}$ , subsequent tests showed that this model overfits and is unable to scale to larger problem instances.

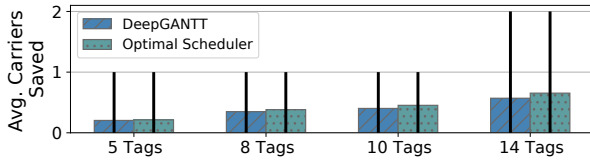
**Model selection.** Based on these findings, we select a 12 GNN-Block Inference Module as final NN model for DeepGANNTT. We generate 520000 random problem instances following the Unique data-generation strategy and train the model according to Sec. V-D using an NVIDIA Titan RTX (requiring only  $\sim 3000$  MiB of GPU memory) for 131 epochs (or 14.6 hours) before reaching the early-stop condition. The model achieves 99.56% accuracy, a carrier-class F1-score of 98.51% and a percentage of correctly computed schedules of  $S_{corr} = 99.43\%$ .

## VI. PERFORMANCE EVALUATION

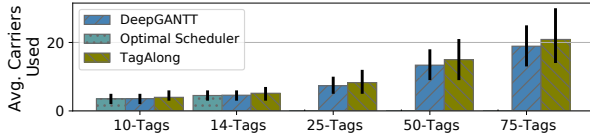
After determining an adequate data-generation strategy and NN architecture for DeepGANNTT in Section V, in this section, we compare DeepGANNTT’s results to those of TagAlong [10] and the optimal scheduler.

We make the following key findings in our evaluation:

- DeepGANNTT performs within 3% of the optimal scheduler on average number of carriers, while consistently outperforming TagAlong by up to 50%. This translates into energy and spectrum savings for the IoT network.
- Our scheduler scales far beyond the problem sizes where it was trained, while still outperforming TagAlong; therefore enabling large resource savings well beyond the limits of the optimal scheduler.
- With a maximum observed computation time of 1.49 s, DeepGANNTT’s speed is comparable to TagAlong’s, and well within the needs of a practical system.



(a) *DeepGANTT performs very close to the optimal scheduler in the range of data sizes seen in training.* Comparison of the average number of carriers saved by DeepGANTT and the optimal scheduler relative to TagAlong.



(b) *DeepGANTT scales far beyond the range of data where the optimal schedules used in training are available, while outperforming TagAlong by a growing margin.* Average number of carriers used. DeepGANTT requires increasingly less carriers than TagAlong.

Fig. 5: Comparison of the carrier-saving performance of DeepGANTT and the optimal scheduler relative to TagAlong for 10 IoT nodes and varying number of tags. The black bars depict the 10 and 90 percentiles.

### A. Carriers saved

Savings in the number of scheduled carrier generation slots have the most impact in terms of spectrum and energy savings for the IoT network. We evaluate the carrier savings achieved with each of the schedulers relative to the TagAlong scheduler. Specifically, for every evaluation problem instance we compute DeepGANTT’s saved carriers as  $C_d - C_t$  and, those of the optimal scheduler as  $C_o - C_t$ ; where  $C_d$ ,  $C_t$ , and  $C_o$  are the number of carriers scheduled by the DeepGANTT, TagAlong and the optimal schedulers respectively.

Fig. 5a shows the average number of carriers saved compared to TagAlong (higher is better) for various network sizes. DeepGANTT’s performance is very close to that of the optimal scheduler in all cases. Note that this range of network sizes overlaps with that on which DeepGANTT was trained.

**Scalability Properties.** We now analyze the capabilities of DeepGANTT in computing schedules for problem sizes well beyond those observed during training. The ability to scale this way directly translates into better scalability than that of the optimal scheduler. Fig 5b shows a comparison of the average number of scheduled cases (lower is better) on problem sizes beyond those used in training. DeepGANTT is able to compute schedules for the 10 tags and 14 tags cases (largest size seen in training) that are nearly equivalent to the Optimal Scheduler. More importantly, DeepGANTT continues to outperform TagAlong by a growing margin well beyond the maximum size of optimal solutions seen in training.

Fig. 8 depicts the number of carriers saved and the percentage of correctly computed schedules  $S_{corr}$  for different network size configurations. We compute schedules for 1000 problem instances for each combination of number of nodes and tags. DeepGANTT consistently increases the mean number of carriers saved as the number of tags increases for all considered configurations. While there are cases where

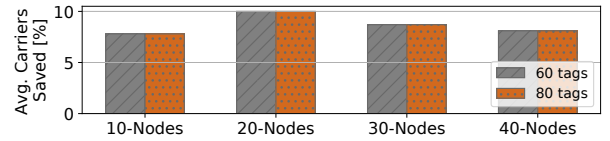


Fig. 6: *DeepGANTT maintains an average saving of almost 10% in scheduled carriers while scaling up to four times the maximum training network size.* Average percentage of carriers saved by DeepGANTT compared to TagAlong for various topology sizes and numbers of tags.

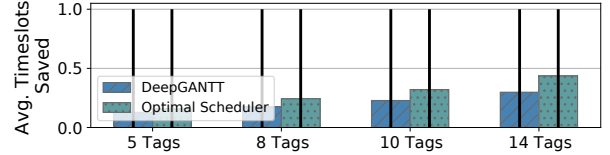


Fig. 7: *DeepGANTT largely mimics the optimal scheduler in timeslots saved, underperforming only slightly.* TagAlong outperforms DeepGANTT in a mere 1.8% of the test set cases. Comparison of the average timeslot savings of DeepGANTT and the optimal scheduler relative to TagAlong for 10 IoT nodes and varying number of tags. The black bars depict the 10 and 90 percentiles.

TagAlong outperforms DeepGANTT, these are actually rare occurrences; this is made clear by the positive mean and the location of the 25-percentiles. Additionally, DeepGANTT’s percentage of correctly-computed schedules ( $S_{corr}$ ) decreases for the 10-node 80-tags case, but remains above 99% for the 30 nodes and 40 nodes problem instances, for all the number of tags considered.

Compared to TagAlong, DeepGANTT is able to reduce the percentage of necessary carriers  $\sim 7\% - 10\%$  on average for large numbers of tags, as depicted in Fig. 6. DeepGANTT is able to reduce the number of carriers by up to 50% for all number of nodes configurations in Fig 8.

### B. Timeslots saved

The number of timeslots in the schedule is the secondary objective in the tag scheduling problem; this is because, while the duration of the schedule can impact latency and other performance metrics in the network, the number of carriers directly impacts energy and spectral efficiency. Note that reducing the number of carrier slots, can potentially also shorten the schedule owing to carrier reuse [11]. We compute the timeslots savings in a manner analogous to the carrier savings and compare with the other schedules in a similar way as depicted in Fig. 7. DeepGANTT largely mimics the performance of the optimal scheduler regarding timeslot savings. TagAlong only outperforms Our scheduler in 1.8% of the test-set instances and always by just one timeslot.

### C. Computation time

The final factor that determines the real-world applicability of a scheduler is the computation time. Fig. 9 depicts a run time comparison of DeepGANTT and TagAlong. While TagAlong runs faster, the absolute values are so small that the difference is negligible in practice. Note that for the largest problem instances considered (40 nodes and 80 tags), the maximum recorded runtime recorded was 1.49s, with an average runtime of 0.25s. This is in stark contrast with



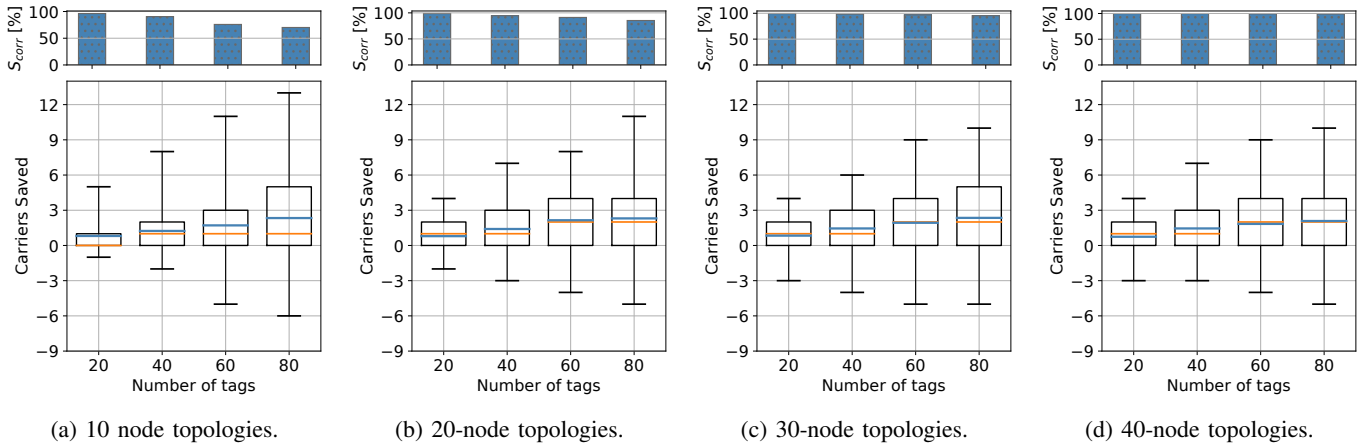


Fig. 8: *DeepGANTT outperforms TagAlong even when increasing the topology sizes far beyond those seen on training.* Scaling capabilities of DeepGANTT when compared to the TagAlong heuristic in terms of carrier savings. The model achieves a maximum carrier reduction of up to 56.1%, 42.3%, 40.0%, 47.4% for 80 tags and 10, 20, 30, and 40 nodes, respectively. The blue and the orange line represent the mean and the median, respectively. Box extents delimit 25 and 75 percentiles. Whiskers delimit 1 and 99 percentiles. The model also has a high success rate ( $S_{corr}$ ), specially for larger topologies.

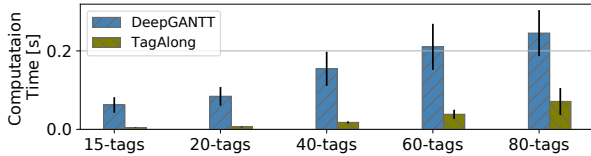


Fig. 9: *While TagAlong runs faster than DeepGANTT, both run times are so small that the difference is negligible.* Run time comparison of DeepGANTT and TagAlong for 10 IoT nodes and various numbers of tags. The black bars represent the standard deviation.

the optimal scheduler that can take several hours to compute schedules for just 10 nodes and 14 tags.

## VII. RELATED WORK & DISCUSSION

Our work is relevant both for scheduling in backscatter networks and for supervised ML applied to communications; in particular, to those of a combinatorial nature.

Many recent related efforts advance backscatter communications and battery-free networks [5]–[8], [29]–[34], but few of these address the efficient provision of unmodulated carriers. Pérez-Penichet et al. demonstrate TagAlong, a complete system with a polynomial-time heuristic to compute interrogation schedules for backscatter devices [10], [11]. Like our work, TagAlong exploits knowledge of the structural properties of the wireless network for fast scheduling. However, TagAlong’s carefully designed algorithm produces wasteful suboptimal schedules. Van Huynh et al. [35] employ numerical analysis to optimize RF energy harvesting tags. By contrast, our work focuses on communication aspects and remains independent of the energy harvesting modality. Carrier scheduling resembles the Reader Collision Problem in RFID systems [36]–[38] in that both need to avoid carrier collisions. These works focus on the monostatic backscatter configuration (where the carrier generator and receiver are co-located), our work focuses on the bi-static configuration (separated carrier generators and receivers). The bi-static configuration leads to a different optimization problem and our focus is on resource optimization rather than mere collision avoidance.

Previous efforts in communications employ reinforcement learning with GNNs to solve combinatorial scheduling problems, mostly on fixed-size networks or static environments [39]–[41]. By contrast our work focuses on a single solution tackling variable-size inputs and outputs, adequate for a multitude of varying conditions. Also novel in our work is that we employ supervised ML to solve the COP; to the best of our knowledge, this is a new approach within backscatter communications. Yet another novelty in our work is our strategy of restricting the solution space of the combinatorial problem to boost the trained model’s performance and scalability properties. ML methods have been applied COPs over graphs in the past years [42], for both reinforcement [43], [44] and supervised learning [45], [46]. Similar to our work, Vinyals et al. [45] implement an attention-based sequence-to-sequence model that learns from optimal solutions and solves the traveling salesman problem. Likewise, Li et al. [46] employ GNNs [20], [47] to solve three traditional COPs with a supervised approach.

Breaking the symmetries in the way we have done, implies that there is a bias in our scheduler: Nodes with lower IDs would deplete their batteries faster, given that they will be selected first as carrier generators. Far from a drawback, we believe that this phenomenon can be exploited at the application level. For instance, one could load-balance carrier scheduling over time, or schedule mains powered carrier generators whenever possible instead of battery-powered ones simply by ordering the IDs in descending order of priority.

Finally, we believe that our approach to deal with multiple solutions in the scheduling problem could have far-reaching implications in solving the broad class of graph-related NP-hard combinatorial problems (such as traveling salesperson) using supervised ML techniques.

## VIII. CONCLUSION

We presents DeepGANTT, a mechanism that employs supervised deep learning to schedule a network of IoT devices interoperating with battery-free backscatter tags. DeepGANTT

leverages self-attention GNNs to overcome the challenges posed by the graph-structured nature of the problem and by variable-size inputs and outputs. Our symmetry-breaking strategies succeed in training DeepGANTT to mimic the behavior of an optimal scheduler.

DeepGANTT exhibits strong generalization capabilities to problem instances up to four times larger than those used in training and can compute schedules, requiring on average 7 – 10% and up to 50% fewer carriers than an existing, carefully crafted heuristic, even for the largest problem instances considered. More importantly, our scheduler performs within 3% of the optimal on the average number of carrier slots while lowering computation times from hours to fractions of a second. With all this, our work advances the development of practical and more efficient backscatter networks.

#### ACKNOWLEDGMENT

This work is financially supported by the Swedish Foundation for Strategic Research (SSF), and by the AIEDGE project by the European Union’s Horizon 2020 research and innovation program (grant agreement No. 101015922).

#### REFERENCES

- [1] V. Liu et al., “Ambient Backscatter: Wireless Communication out of Thin Air,” in *Proc. Special Interest Group Data Commun. (SIGCOMM)*, ACM, 2013, pp. 39–50.
- [2] A. Wang et al., “FM Backscatter: Enabling Connected Cities and Smart Fabrics,” in *NSDI’17*. USENIX, 2017, pp. 243–258.
- [3] M. Hessar, A. Najafi, and S. Gollakota, “Netscatter: Enabling large-scale backscatter networks,” in *NSDI’18*. USENIX, 2018.
- [4] B. Kellogg et al., “Passive Wi-Fi: Bringing Low Power to Wi-Fi Transmissions,” in *NSDI’16*, 2016, p. 151.
- [5] J. Ensworth and M. S. Reynolds, “Every smart phone is a backscatter reader: Modulated backscatter compatibility with Bluetooth 4.0 Low Energy (BLE) devices,” in *Proc. Ann. Conf. RFID*. IEEE, 2015.
- [6] B. Kellogg et al., “Wi-Fi Backscatter: Internet Connectivity for RF-powered Devices,” in *Proc. Special Interest Group Data Commun. (SIGCOMM)*. New York, NY, USA: ACM, 2014, pp. 607–618.
- [7] V. Talla, M. Hessar, B. Kellogg, A. Najafi, J. R. Smith, and S. Gollakota, “LoRa Backscatter: Enabling The Vision of Ubiquitous Connectivity,” vol. 1, no. 3, Sep. 2017, pp. 105:1–105:24.
- [8] V. Iyer et al., “Inter-Technology Backscatter: Towards Internet Connectivity for Implanted Devices.” ACM, 2016, pp. 356–369.
- [9] C. Pérez-Penichet, F. Hermans, A. Varshney, and T. Voigt, “Augmenting IoT networks with backscatter-enabled passive sensor tags,” in *Proc. Annu. Int. Conf. Mobile Comput. Netw. (MOBICOM)*. ACM, oct 2016, pp. 23–27.
- [10] C. Pérez-Penichet, D. Piumwardane, C. Rohner, and T. Voigt, “TagA-long: Efficient Integration of Battery-Free Sensor Tags in Standard Wireless Networks,” in *Proc. 19th ACM/IEEE Int. Conf. Inf. Process. Sensor Netw. (IPSN)*, Sydney, Australia, 2020.
- [11] C. Pérez-Penichet, D. Piumwardane, C. Rohner, and T. Voigt, “A Fast Carrier Scheduling Algorithm for Battery-free Sensor Tags in Commodity Wireless Networks,” in *Proc. Int. Conf. Comput. Commun. (INFOCOM)*. IEEE, 2020, pp. 994–1003.
- [12] C. Pérez-Penichet, C. Noda, A. Varshney, and T. Voigt, “Battery-Free 802.15.4 Receiver,” in *Proc. 17th ACM/IEEE Int. Conf. Inf. Process. Sensor Netw. (IPSN)*. IEEE, 2018, pp. 164–175.
- [13] IEEE, *IEEE Standard for Low-Rate Wireless Networks –Amendment 2: Ultra-Low Power Physical Layer*, Apr. 2016.
- [14] Bluetooth SIG, *Bluetooth Core Specification 5.3*, 2021.
- [15] J. L. Ba, J. R. Kiros, and G. E. Hinton, “Layer Normalization,” in *Proc. Advances NIPS 2016 Deep Learn. Symp.* NIPS, jul 2016.
- [16] A. Vaswani, N. Shazeer, N. Parmar, J. Uszkoreit, L. Jones, A. N. Gomez, Ł. Kaiser, and I. Polosukhin, “Attention is all you need,” in *Proc. Advances Neural Inf. Process. Syst. (NIPS)*, vol. 2017-Decem. NIPS, jun 2017, pp. 5999–6009.
- [17] Y. Shi, Z. Huang, S. Feng, H. Zhong, W. Wang, and Y. Sun, “Masked Label Prediction: Unified Message Passing Model for Semi-Supervised Classification,” Tech. Rep., 2021.
- [18] W. L. Hamilton, R. Ying, and J. Leskovec, “Inductive Representation Learning on Large Graphs,” in *Proc. Advances Neural Inf. Process. Syst. (NIPS)*, vol. 2017-Decem. Neural information processing systems foundation, jun 2017, pp. 1025–1035.
- [19] P. Veličković, A. Casanova, P. Liò, G. Cucurull, A. Romero, and Y. Bengio, “Graph attention networks,” in *Proc. 6th Int. Conf. Learn. Representations (ICLR)*. ICLR, oct 2018.
- [20] T. N. Kipf and M. Welling, “Semi-Supervised Classification with Graph Convolutional Networks,” in *Proc. 5th Int. Conf. Learn. Representations (ICLR)*. ICLR, sep 2017.
- [21] A. A. Hagberg, D. A. Schult, and P. J. Swart, “Exploring network structure, dynamics, and function using networkx,” in *Proceedings of the 7th Python in Science Conference*, G. Varoquaux, T. Vaught, and J. Millman, Eds., Pasadena, CA USA, 2008, pp. 11 – 15.
- [22] N. Nethercote, P. J. Stuckey, R. Becket, S. Brand, G. J. Duck, and G. Tack, “MiniZinc: Towards a standard CP modelling language,” in *Lecture Notes in Computer Science*, vol. 4741 LNCS. Springer Verlag, 2007, pp. 529–543.
- [23] L. Perron and V. Furnon, “Or-tools,” Google. [Online]. Available: <https://developers.google.com/optimization/>
- [24] A. Paszke, S. Gross, F. Massa, A. Lerer, J. Bradbury, G. Chanan, and et al., “Pytorch: An imperative style, high-performance deep learning library,” in *Proc. Advances Neural Inf. Process. Syst.*, H. Wallach, H. Larochelle, A. Beygelzimer, F. d’Alché-Buc, E. Fox, and R. Garnett, Eds. Curran Associates, Inc., 2019, pp. 8024–8035.
- [25] M. Fey and J. E. Lenssen, “Fast graph representation learning with PyTorch Geometric,” in *Proc. ICLR Workshop Representation Learn. Graphs Manifolds*, 2019.
- [26] D. P. Kingma and J. Lei Ba, “Adam: A method for stochastic optimization,” in *Proc. Int. Conf. Learn. Representations (ICLR)*, 2015.
- [27] J. You, R. Ying, and J. Leskovec, “Position-aware Graph Neural Networks,” in *Proc. 36th Int. Conf. Mach. Learn. (ICML)*, 2019.
- [28] V. P. Dwivedi, C. K. Joshi, T. Laurent, Y. Bengio, and X. Bresson, “Benchmarking Graph Neural Networks,” Tech. Rep., mar 2020.
- [29] B. Kellogg et al., “Passive Wi-Fi: Bringing Low Power to Wi-Fi Transmissions,” in *Proc. Symp. Networked Syst. Des. Implementation (NSDI)*. NSDI, 2016, pp. 151–164.
- [30] P. Zhang, C. Josephson, D. Bharadia, and S. Katti, “FreeRider: Backscatter Communication Using Commodity Radios,” ser. CoNEXT ’17. Incheon, Republic of Korea: ACM, 2017, pp. 389–401.
- [31] A. Y. Majid, M. Jansen, G. O. Delgado, K. S. Yildirim, and P. Pawełczak, “Multi-hop backscatter tag-to-tag networks,” in *Proc. Int. Conf. Comput. Commun. (INFOCOM)*. IEEE, April 2019, pp. 721–729.
- [32] P. V. Nikitin, S. Ramamurthy, R. Martinez, and K. V. S. Rao, “Passive tag-to-tag communication,” in *Proc. Int. Conf. RFID (RFID)*. IEEE, April 2012, pp. 177–184.
- [33] Y. Karimi, A. Athalye, S. R. Das, P. M. Djurić, and M. Stanačević, “Design of a backscatter-based tag-to-tag system,” in *2017 IEEE International Conference on RFID (IEEE RFID)*, May 2017, pp. 6–12.
- [34] K. Geissdoerfer and M. Zimmerling, “Bootstrapping Battery-free Wireless Networks: Efficient Neighbor Discovery and Synchronization in the Face of Intermittency,” in *NSDI’21*, 2021, pp. 439–455.
- [35] N. V. Huynh, D. T. Hoang, D. Niyato, P. Wang, and D. I. Kim, “Optimal time scheduling for wireless-powered backscatter communication networks,” *IEEE Wireless Commun. Lett.*, vol. 7, pp. 820–823, 2018.
- [36] L. Yang, J. Han, Y. Qi, C. Wang, T. Gu, and Y. Liu, “Season: Shelving interference and joint identification in large-scale RFID systems,” in *Proc. Int. Conf. Comput. Commun. (INFOCOM)*. IEEE, April 2011, pp. 3092–3100.
- [37] E. Hamouda, N. Mitton, and D. Simplot-Ryl, “Reader Anti-collision in dense RFID networks with mobile tags,” in *2011 IEEE International Conference on RFID-Technologies and Applications*, Sep. 2011, pp. 327–334.
- [38] H. Yue, C. Zhang, M. Pan, Y. Fang, and S. Chen, “A time-efficient information collection protocol for large-scale RFID systems,” in *Proc. Int. Conf. Comput. Commun. (INFOCOM)*. IEEE, March 2012, pp. 2158–2166.
- [39] F. Wang, C. Zhang, F. Wang, J. Liu, Y. Zhu, H. Pang, and L. Sun, “Intelligent Edge-Assisted Crowdcast with Deep Reinforcement Learning for Personalized QoE,” in *Proc. IEEE Int. Conf. Comput. Commun. (INFOCOM)*, vol. 2019-April. IEEE, apr 2019, pp. 910–918.

- [40] H. Zhang, W. Li, S. Gao, X. Wang, and B. Ye, "ReLeS: A Neural Adaptive Multipath Scheduler based on Deep Reinforcement Learning," in *Proc. Int. Conf. Comput. Commun. (INFOCOM)*, vol. 2019-April. IEEE, apr 2019, pp. 1648–1656.
- [41] R. Bhattacharyya, A. Bura, D. Rengarajan, M. Rumuly, S. Shakkottai, D. Kalathil, R. K. P. Mok, and A. Dhamdhere, "QFlow: A Reinforcement Learning Approach to High QoE Video Streaming over Wireless Networks." ACM, jan 2019, pp. 251–260.
- [42] N. Vesselinova, R. Steinert, D. F. Perez-Ramirez, and M. Boman, "Learning combinatorial optimization on graphs: A survey with applications to networking," *IEEE Access*, vol. 8, pp. 120 388–120 416, 2020.
- [43] H. Dai, E. B. Khalil, Y. Zhang, B. Dilkina, and L. Song, "Learning Combinatorial Optimization Algorithms over Graphs," in *Proc. Advances Neural Inf. Process. Syst. (NIPS)*, vol. 2017-Decem. Neural information processing systems foundation, apr 2017, pp. 6349–6359.
- [44] S. Manchanda, A. Mittal, A. Dhawan, S. Medya, S. Ranu, and A. Singh, "Learning Heuristics over Large Graphs via Deep Reinforcement Learning," in *Proc. 34th Conf. Neural Inf. Process. Syst. (NIPS)*, mar 2020.
- [45] O. Vinyals, G. Brain, M. Fortunato, and N. Jaitly, "Pointer Networks," in *Proc. Advances Neural Inf. Process. Syst. (NIPS)*, 2015, pp. 2692–2700.
- [46] Z. Li, Q. Chen, and V. Koltun, "Combinatorial optimization with graph convolutional networks and guided tree search," in *Proc. Advances in Neural Inf. Process. Syst. (NeurIPS)*, 2018, pp. 539–548.
- [47] M. Defferrard, X. Bresson, and P. Vandergheynst, "Convolutional Neural Networks on Graphs with Fast Localized Spectral Filtering," in *Proc. Advances in Neural Inf. Process. Syst. (NeurIPS)*. NeurIPS, jun 2016, pp. 3844–3852.